Experimental fluence modulated proton computed tomography by pencil beam scanning

George Dedes[1], Robert P. Johnson[2], Mark Pankuch[3], Nick Detrich[3], Willemijn M. A. Pols[1], Simon Rit[4], Reinhard W. Schulte[5], Katia Parodi[1], Guillaume Landry[1]

[1]*Department of Medical Physics, Faculty of Physics, Ludwig-Maximilians-Universität München (LMU Munich), 85748 Garching b. München, Germany*

[2]*Department of Physics, U.C. Santa Cruz, Santa Cruz, CA 95064, USA*

[3]*IBA and Northwestern Medicine Chicago Proton Center, Warrenville, 60555 IL, USA*

[4]*Université de Lyon, CREATIS, CNRS UMR5220m Inserm U1044, INSA-Lyon, Université Lyon 1, F69373 Lyon, France*

[5]*Division of Radiation Research, Loma Linda University, Loma Linda, CA 92354, USA*

Submitted to: Medical Physics

Short title: Experimental FMpCT

Number of pages: 26

Number of figures: 10

Number of tables: 1

Corresponding author: George Dedes, g.dedes@lmu.de

Abstract

Purpose

This experimental study is aimed at demonstrating, using a simple cylindrical water phantom, the feasibility of fluence modulated proton computed tomography (FMpCT) by pencil beam scanning (PBS) proton computed tomography (pCT).

Methods

The phase II pCT prototype of the Loma Linda U. and U. C. Santa Cruz was operated using the PBS beam line of the Northwestern Medicine Chicago Proton Center. A 20x10 grid of 1.37 cm full width half maximum pencil beams (PB) equally spaced by 1 cm was used to acquire 45 projections in step and shoot mode. The PB pattern's fluence was modified to allow FMpCT scans with fluence modulation factors (FMF) of 50% and 20%. A central FMpCT region of interest (FMpCT-ROI) was used. Reconstructed images were evaluated in terms of relative stopping power (RSP) accuracy and noise using annular ROIs. The FMpCT dose savings were estimated by Monte Carlo (MC) simulation of the pCT acquisitions using beam phase space distributions. PBS pCT results with homogeneous fluence were additionally compared to broad beam results in terms of RSP accuracy and noise.

Results

PBS pCT scans with acceptable pile-up were possible, and images were comparable to previously acquired broad beam pCT images in terms of both noise and accuracy. In the FMpCT-ROI, the noise and accuracy from full fluence (FF) scans were preserved. Dose savings of up to 60% were achieved at the object's edge when using FMF of 20%.

Conclusion

In this study, we have demonstrated that PBS pCT scans can achieve equivalent accuracy as those obtained from broad beams. The feasibility of FMpCT scans was demonstrated; image accuracy and noise were successfully preserved in the central FMpCT-ROI chosen for this study, and dose reduction of up to 60% at the object's edge was realized.

Word count: 290/300

1. INTRODUCTION

The use of x-ray computed tomography (CT) scans for relative (to water) proton stopping power (RSP) estimation, a quantity necessary for dose calculation, contributes considerably to range uncertainties in proton therapy[1,2]. The potential of reducing these uncertainties by direct RSP measurements at the treatment table has motivated the recent revival of proton computed tomography (pCT), which was first proposed by Cormack in the early 1960s[3]. By measuring protons' positions and residual energies behind the patient in a series of projections, a RSP image can be reconstructed[4-8]. Currently, several groups are known to be designing, building or operating pCT (or heavier ion CT) prototypes[9-13] and initial reports of RSP accuracy are encouraging[14].

The eventual use of pCT for frequent imaging in treatment position is supported by the fact that pCT dose efficiency, evaluated by metrics such as contrast to noise ratio, is superior to x-ray CT[15] and may allow lower imaging doses. Recently, pCT scans using imaging doses as low as 1 mGy have been achieved[10]. The imaging dose from pCT may be further reduced by employing the concept of fluence field modulation[16-23], where the fluence of particles used for imaging is adjusted within a projection to yield spatially varying image quality. For proton therapy guided by pCT, we could thus envision imaging the therapeutic beam paths with high image quality (low noise) and sacrificing image quality (high noise) where therapy related dose computation is not required. This is particularly attractive for proton therapy given the low integral dose nature of the modality[24]. A recent simulation study suggested that fluence modulated pCT (FMpCT) may yield imaging dose reduction of 30% and 50% in head-and-neck and brain cancer

patients respectively, while preserving the dose calculation accuracy of a full fluence image[25].

FMpCT may be achieved by acquiring pCT scans using the pencil beam scanning (PBS) functionality of modern proton therapy facilities instead of the broad beams (cone or wobbled beams typically) currently employed in most pCT prototypes[10]. The use of PBS would greatly simplify the fluence modulation task by allowing the prescription of proton fluence on a pencil beam by pencil beam basis. PBS scans have been previously acquired for carbon ion CT[26,27] with an integrating detector, which functions in PBS mode by design, benefitting from the straighter paths of carbon ions[9]. Helium CT results obtained from PBS have also been presented for a particle tracking scanner, and the same study reported the acquisition of PBS pCT as well, but no results were reported[28].

In this study, we performed PBS pCT scans and first experimental realization of FMpCT by making use of the Phase II preclinical prototype pCT scanner of the Loma Linda University and U.C. Santa Cruz, together with the PBS capability of the Northwestern Medicine Chicago Proton Center. Our aim was to demonstrate the equivalence, in terms of image quality, of PBS and broad beam acquisitions, and the feasibility of FMpCT using a simple water cylinder phantom with a centrally located FMpCT region of interest (FMpCT-ROI) for high image quality. Specifically, this work aimed at demonstrating that 1) PBS pCT can achieve the same image quality as cone beam or wobbled beam pCT in uniform fluence scenarios and 2) that FMpCT scans preserving image quality in the FMpCT-ROI are feasible with PBS pCT.

2. MATERIALS AND METHODS

2.1. Experimental setup

The experimental part of this study was performed at the Northwestern Medicine Chicago Proton Center using the Phase II preclinical pCT prototype scanner of the Loma Linda University and U.C. Santa Cruz, described in detail in Johnson et al.[29] The scanner consists of two tracking modules and a 5-stage water-equivalent-path-length (WEPL) detector coupled to a data acquisition system capable of acquiring broad beam proton events at a sustained rate in excess of 1 MHz.

The front and rear tracking modules together contain 32 single-sided silicon strip detectors (SSD) with a strip pitch of 228 μm and 400 μm thickness. Four SSDs are assembled on a printed circuit board (PCB) in a pattern that forms a continuous sensitive area of 8.95×35.6 cm^2. Two back-to-back PCBs with orthogonal orientation form a 2D coordinate detector, and each tracking module consists of two such 2D coordinate detectors. The tracking system therefore provides 4 sets of 3D coordinates, allowing the estimation of the curved proton path using the measured position and direction vector of each proton before and after the object.

The 5-stage plastic scintillating detector has a dynamic range of 0-260 mm WEPL. Each 52 mm thick stage is made of polystyrene of RSP=1.038 and has a lateral area of 10×40 cm^2. The WEPL information for every proton is given by the signal from the stage in which the proton stopped[30].

2.2. PBS beam line

The PBS beam was delivered in a clinically commissioned fixed beam line using a universal nozzle manufactured by IBA. (IBA, Belgium). The accelerator source for this room is an IBA C230 cyclotron that has been in clinical use since 2010 at the Northwestern Medicine Chicago Proton Center. For proton imaging, extremely low proton flux is needed. The standard method of regulating dose using signal from the nozzle's monitor chambers was not feasible due to the very low signal to noise ratio of the imaging beam. Instead, spot dwells were based on a fixed dwell time, which is the beam-on time at a specific position, along with setting the cyclotron output current once to provide the desired total fluence and flux.

2.3. Phantom

For this experimental proof-of-principle work we chose a simple cylindrical water phantom. The phantom is made of a PMMA cylindrical container with inner diameter of 137.8 mm and outer diameter of 150.5 mm. The thickness of the cylinder is 28 mm and the two PMMA endcaps have a thickness of 6 mm each. The container was filled with water and placed on a remotely-controlled rotating stage.

2.4. PBS scan patterns

Proton CT images were acquired using active pencil beam (PB) scanning. A 200 MeV PB with a spot size of 1.37 cm FWHM in air at isocenter was magnetically deflected in order

to cover an area of 30×10 cm^2 in the case of the calibration runs (300 PBs) and 20×10 cm^2 in the case of the imaging scans (200 PBs). The beam was turned off for the duration of the deflection to the next point. Beam spot locations were spaced 1 cm apart. The pencil beam grid was offset by a quarter of the PB spacing in the direction normal to scan's axis of rotation to avoid overlapping PB from opposing projections and thereby improve the measurement uniformity.

2.5. Pile-up study

The pCT Phase II scanner had been so far mostly used with broad proton beams: either a passively scattered cone beam at the Loma Linda University Medical Center[31], covering the whole field of view of the scanner, or at the Northwestern Medicine Chicago Proton Center with a wobbled proton beam of 4 to 7 cm FWHM spot size[10]. The single report of scanner operation in PBS mode makes no mention of pile-up[28]. Before performing the calibration and imaging runs, a study was made on the detector performance for a 1.37 cm FWHM PB, concentrating especially on the resulting pile-up in the silicon strips of the tracker modules. The main concern was that the amplifier time-over-threshold for the silicon strips could be such that if two protons impinge on the same strip within a time window of less than about one microsecond, the second one will be missed.

For the purpose of the pile-up study, a 30×10 cm^2 field (300 PBs) was employed, with the beam running at cyclotron currents of 2, 4, 6, 8, 10 and 12 nA in six different runs and impinging upon the detector without any object in the field of view. The PB dwell time was 8 ms. This dataset was employed to select a suitable cyclotron current, taking into account the trade-off between pile-up and acquisition speed. No formal optimization

was done, however, as a decision for the subsequent runs had to be made within a few minutes.

We have subsequently further analysed the data from these six runs in order to understand the impact of pile-up on the efficiency of individual proton detection in the same PB. The efficiency to detect a proton "hit" in the silicon-strip detectors can be directly measured in a given layer for either of the two views (vertical strips, coordinate V and horizontal strips, coordinate T) by fitting a straight line to the hits in the other three layers to predict where there should be a hit in the layer of interest. With zero pile-up that efficiency is generally found to be above 99%, with most of the loss coming from the gaps between individual silicon wafers[29].

2.6. Calibration run

A calibration procedure that transforms the detector single-proton measurement to WEPL is necessary and is discussed in Bashkirov et al.[30] The pCT collaboration has developed an improved version in which a polystyrene wedge phantom is used[32] instead of the stepped pyramid phantom. In addition to the wedge, four polystyrene blocks are required to bring the proton Bragg peak into each stage of the 5-stage plastic scintillator detector[30].

The calibration was performed at the beginning of a scanning session in five consecutive runs, in addition to an "empty" run made without any object. The wedge provides a continuous WEPL range that is traversed by protons, whose position and hence path

length in the phantom is provided by the tracking system. The first calibration run was acquired with only the wedge, resulting in protons stopping at different depths in the last stage. Four additional runs were acquired by adding every time one block behind the wedge, so that protons stop in each of the four remaining stages. A run with no phantom was also acquired and was used to map the spatial dependence of the scintillator signals as well as to provide a conversion from ADC counts to MeV[30]. The result of the calibration run was a look-up table transforming an energy measurement to the traversed WEPL for a proton stopping in a particular stage. All calibration runs were acquired using a 30×10 cm^2 (300 PBs) field with a cyclotron current of 4 nA with 8 ms dwell time per PB position, with 6 repetitions of the scan pattern.

2.7. pCT scan acquisitions

Each scan consisted of 45 projections, acquired at 8 degree steps, with the phantom rotating between the acquisitions of two consecutive projections (step-and-shoot mode). Following the pile-up study and calibration, a 20x10 cm^2 scanning pattern with 27 ms dwell time delivered in a single pass with a cyclotron current of 4 nA was chosen. This resulted in a 400 kHz counting rate (averaged over a projection).

The fluence of each PB was controlled by changing its dwell time. For the full fluence (FF) scan the dwell time was kept at 27 ms. In that case, the acquisition of a single projection required 7 s, and 2.2 million protons were recorded. For the FMpCT scans, a FMpCT-ROI was imaged with the FF, while for the remaining PBs in the 20×10 cm^2 imaging field, the PB fluence was reduced by 50% (FMpCT50) and 20% (FMpCT20) by reducing the dwell time to 13.5 ms and 5.4 ms, respectively. The central FMpCT-ROI

was defined as the region irradiated by the 5×10 central PBs. An unintentional misalignment caused a shift of 1 cm in the PB scan pattern, resulting in a smaller FMpCT-ROI covered by FF PBs in all projections. The final effective size of the FMpCT-ROI was 3 cm in diameter and 10 cm in height.

2.8. Image reconstruction

Images were reconstructed for this study with a filtered backprojection (FBP) implementation that accounts for the curved proton paths in the imaged object, mainly due to multiple Coulomb scattering. The main principles of the algorithm are presented in Rit et al.[8] The path of every proton is approximated by a most likely path (MLP) formulation (Schulte et al., 2008), which uses the position and direction information from the tracking modules.

Protons were selected with a 3 standard deviations cut on the energy and angular distributions around their mean energy and angle per projection pixel. List-mode data were binned in intermediate projection images with 0.8 mm × 0.8 mm pixels, which were then filtered and back-projected. Sinogram interpolation[4] was used for all reconstructions.

To better understand the noise behaviour outside the FMpCT-ROI, images were additionally reconstructed from homogeneous scans with fluence virtually reduced to 50% and 20% of the FF scan. Those scans were not explicitly acquired during the experiment but were obtained from the FF dataset by assigning a uniform selection probability to every proton.

Finally, the results of the PB pCT scans acquired in this experiment were compared to an older scan of the same phantom imaged with a wobbled proton beam with a size of 4 cm FWHM[10]. For comparability, the wobbled beam scan data were processed so as to contain the same number of protons per projection, and the same number of projections as the FF PB scan.

2.9. RSP noise and accuracy quantification

The image quality of the acquired pCT scans was quantified in terms of RSP accuracy and RSP noise. Utilizing the cylindrical symmetry of the scanned object, the image quality metrics were assessed in annular ROIs with increasing radius, covering different radial extents of the phantom. For comparability, all ROIs contained approximately 1000 pixels, resulting in variable annulus thicknesses. The RSP accuracy in an annulus was defined as the mean value of the RSP distribution of all pixels contained in it, expressed as a percentage difference from the theoretical value for water (RSP=1). The RSP noise in an annulus was defined in a similar manner, using the standard deviation of the RSP distribution. Finally, the inner radius of each annulus denotes the radial distance from the center of the cylindrical phantom. The ROIs are shown in supplementary Figure S1.

2.10. Imaging dose

During the experiment, there was no possibility of dose estimation for each scan. In order to quantify the dose gains of FMpCT with respect to the FF scans, we simulated the dose in the water phantom using Monte Carlo simulations. A full simulation was employed that models in high detail all the active and passive scanner elements. The

simulation application based on Geant4, version 10.02.p1, was presented in Giacometti et al.[14] The dose in the water phantom was estimated by a Geant4 primitive dose scorer in a 1×1×1 mm^3 voxel grid using a proton phase space distribution estimated from the front tracking module. The resulting dose distributions were normalized to the FF scan to estimate dose savings from FMpCT. Absolute doses were however not reported.

3. RESULTS

3.1 Evaluation of pile-up with pencil beam scanning

Figure 1 shows the efficiency measurements resulting from the pencil-beam runs. The highest trigger rate of 910 kHz is only about 30% below the maximum event rate that the data acquisition can sustain. At the data rate (400 kHz) employed in the experiments described below, the hit inefficiency caused by pile-up is only about 1% and is thus negligible.

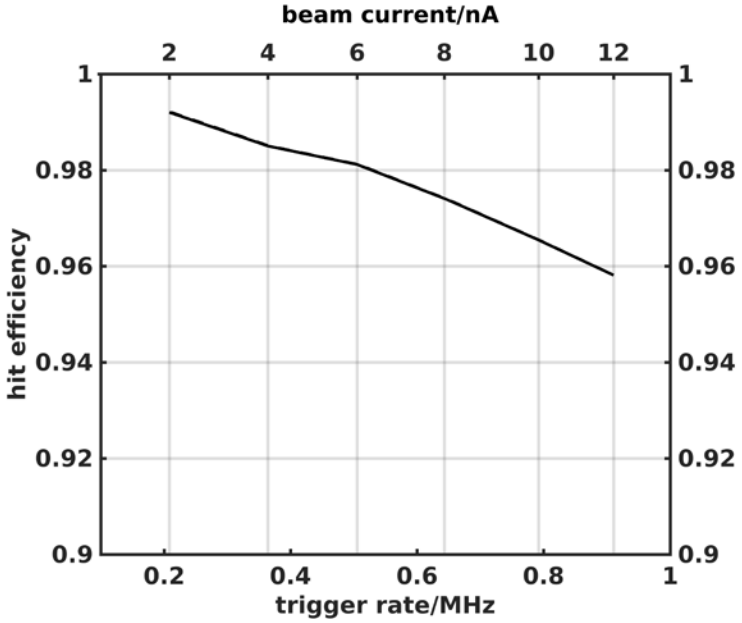

Figure 1. The measured hit efficiency averaged over all eight tracker layers versus the trigger rate. The falloff in efficiency with increasing rate is due to pile-up in the amplifiers of the silicon-strip detectors.

Figure 2 shows the fraction of events for which a proton track could be reconstructed along the vertical and transverse directions as a function of the trigger rate corresponding to the different cyclotron currents considered. We observed an increase in pile-up with increasing current, with the tracking efficiency dropping from 90% at 2 nA

and 200 kHz to 85% at 12 nA and 900 kHz. The remainder of the experiments and the results presented in this section were obtained with 4 nA and a trigger rate of 400 kHz.

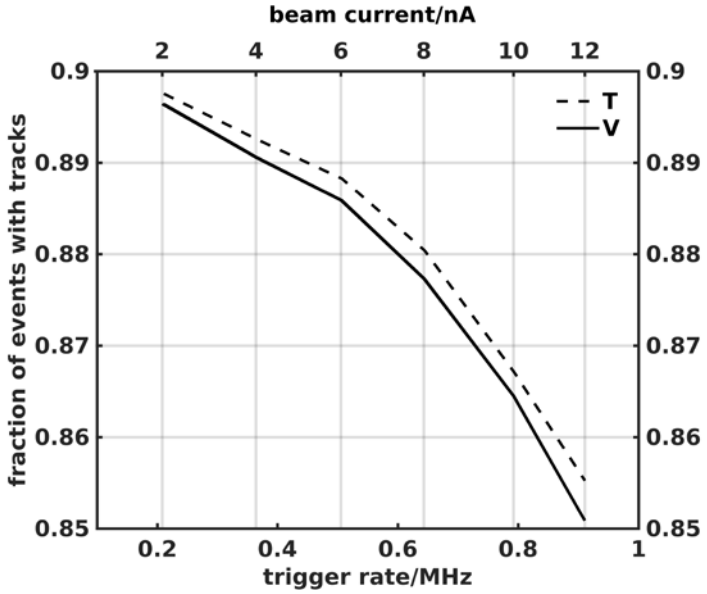

Figure 2. The fraction of triggered events for which proton tracks in the vertical (V) and transverse (T) directions could be obtained as a function of the trigger rate or cyclotron current.

3.2 Comparison to established imaging with wobbled delivery

Figure 3 shows the detector's stage-wise energy-to-WEPL calibration curves obtained with an open field using the wobbled beam and PBS. The curves nearly overlap, indicating that the PBS and wobbled beam calibrations are equivalent.

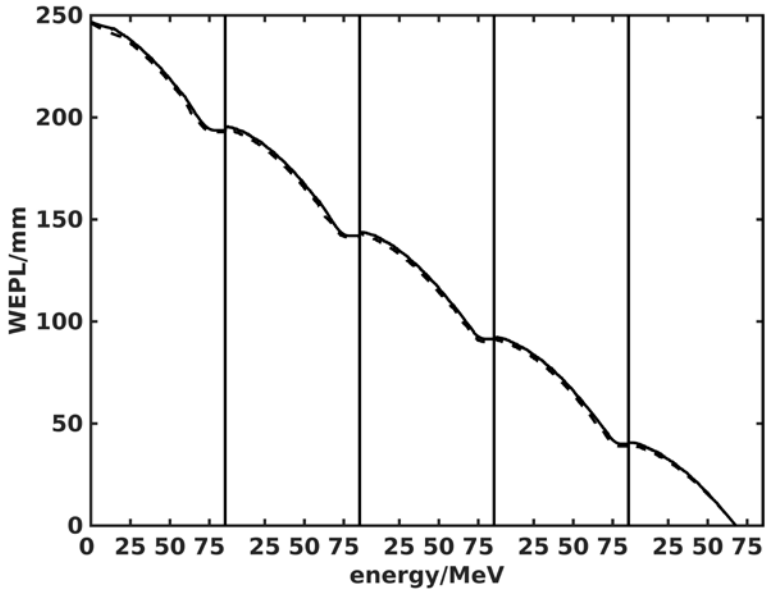

Figure 3. Calibration plots for the five consecutive energy detector stages based on the wobbled (dashed line) and pencil beam scanning (solid line) beams. The horizontal scale refers to the energy deposition in the stage in which the proton apparently stopped

Figure 4 shows reconstructed pCT images from full fluence scans of the water cylinder phantom acquired with a wobbled beam and with pencil beam scanning. The images are generally similar, with the wobbled beam exhibiting a slightly darker artefact at the centre of the water cylinder. Using a ROI covering 90% of the water cylinder's radius, the mean (standard deviation) of the water RSP were 1.011 (0.053) and 0.993 (0.049) for the wobbled and pencil beams, respectively. Figure 5 makes use of annular ROIs (see supplementary figure S1) to present the RSP accuracy and noise. We observed that the pencil beam scanning images had better accuracy (results closer to 0% error), and that the difference between the wobbled and PBS images was limited to about 1%. Both images showed increasing noise with radius. There was good agreement between the

noise levels in the centre of the cylinder but slightly higher values for the wobbled beam were observed at the object's edge.

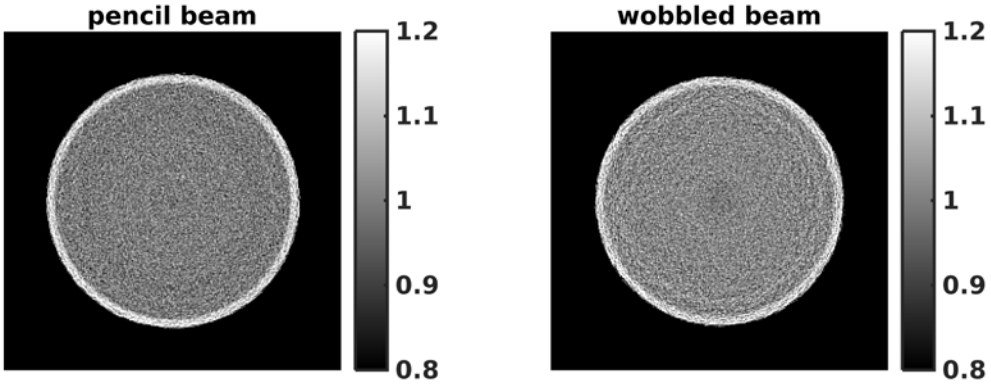

Figure 4. pCT images (image values are RSP) acquired with pencil beam scanning and a wobbled beam.

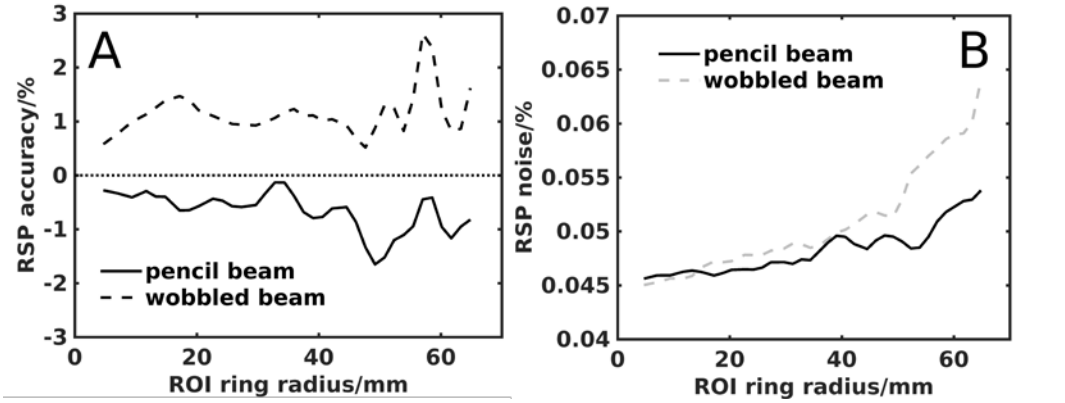

Figure 5. (A) Error on mean RSP of water estimated using annular ROIs in pCT images acquired with pencil beam scanning and a wobbled beam. (B) Corresponding standard deviation (noise).

3.3 FMpCT

Figure 6 presents the front tracker proton counts showing the pencil beam fluence used for each projection of the FF and FMpCT scans. Individual pencil beams are resolvable as well as the quarter detector shift employed to increase the in-slice dose uniformity. We

observed that due to an experimental misalignment of the pencil beam scanning system and the phantom's rotation stage, the high fluence region (5 PBs) was shifted by one pencil beam. We also noticed a slight horizontal tilt attributed to the scanner not being perfectly level. The pattern of darker lines is attributed to gaps between active tracker elements.

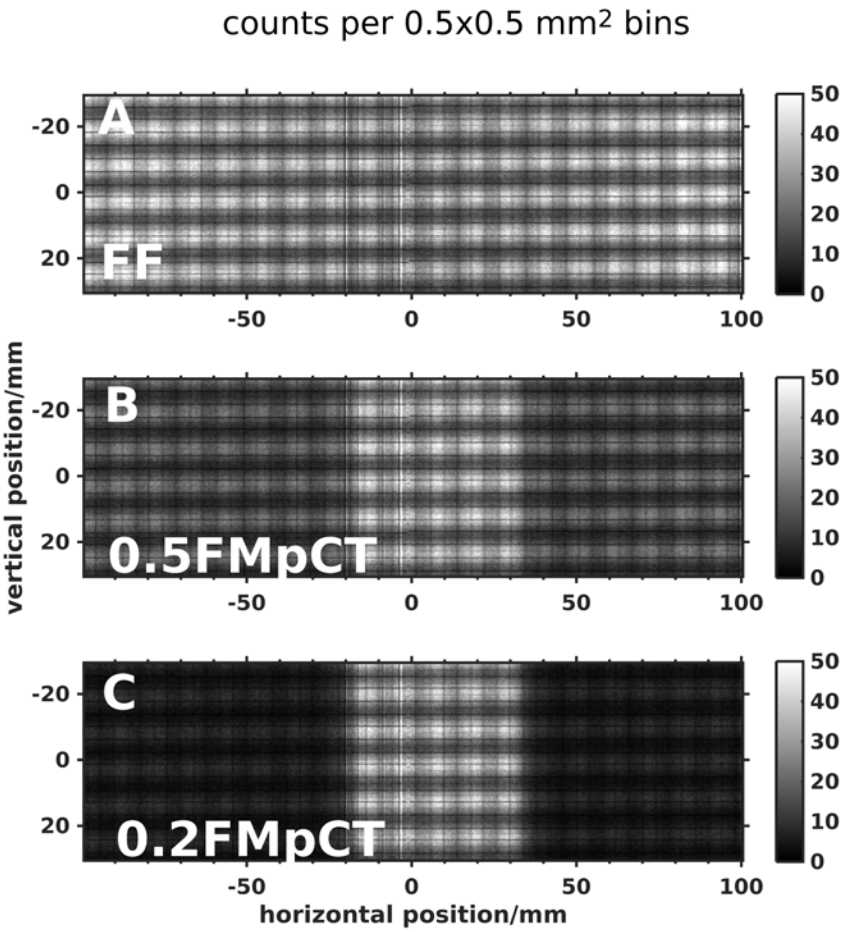

Figure 6. Front tracker proton counts for (A) full fluence (FF), (B) FMpCT with FMF 0.5 and (C) 0.2. The horizontal axis is parallel to the cylindrical phantom's diameter and the vertical axis is parallel to the phantom's rotation axis.

Figure 7 presents the reconstructed PBS pCT images for varying levels of uniform fluence as well as FMpCT images with FMF of 0.5 and 0.2. The expected increase of noise with lower proton fluence was observed for uniform fluence images, while with FMpCT the image quality in the centre of the phantom appears qualitatively preserved while the noise at the object's edge tends to approach the uniform fluence scenario.

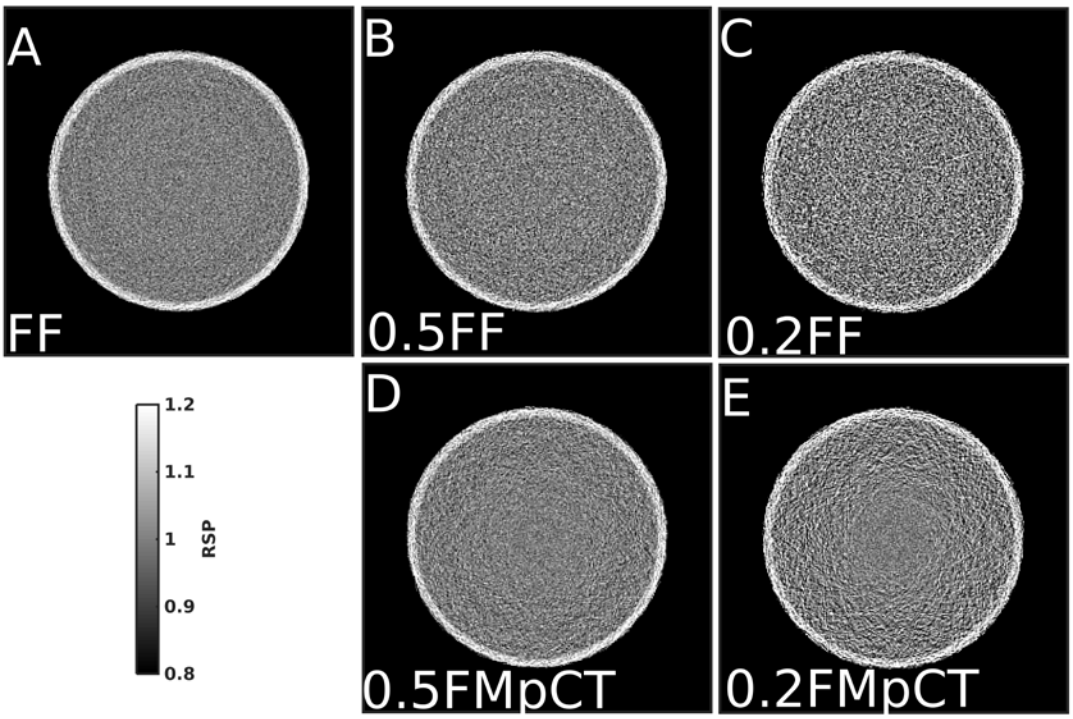

Figure 7. PBS pCT RSP images with (A) homogeneous full fluence (FF) and reduced uniform fluence by factors (B) 0.5 and (C) 0.2. (D,E) PBS FMpCT RSP images with FMF of (D) 0.5 and (E) 0.2.

This finding was quantified in Figure 8, where the standard deviation in the annular ROIs is reported for the images presented in Figure 7. We can observe that in the low noise ROI the standard deviation of the FMpCT images matches the one obtained from the FF image, while the uniform low fluence images have overall higher noise. For FMpCT

images, the noise increases rapidly with the distance from the ROI, approaching the uniform fluence cases at the edge of the object.

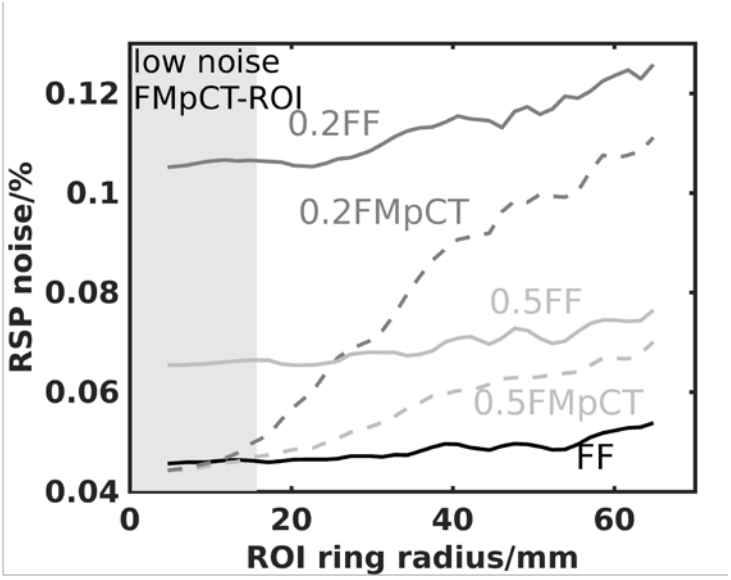

Figure 8. Standard deviation (noise) of RSP of water estimated from pCT images using annular ROIs. The extent of the FMpCT-ROI is indicated in grey.

Figure 9 reports the RSP error (for water) of the mean values for the uniform FF and FMpCT images in the annular ROIs. We see that the use of FMpCT with FMF 0.5 does not alter the RSP accuracy inside and outside the low noise ROI. A slight variation of accuracy for FMF 0.2 was observed in the low noise FMpCT-ROI. This can be observed in Table 1 where we see that the mean value in the case of FMpCT with FMF 0.2 is 0.2% lower than in the corresponding uniform fluence case.

Table 1. Mean RSP noise and standard deviation in the FMpCT-ROI. The second column shows RSP mean values for uniform scans with different FMF. The third column reports mean values with FMpCT. The fourth and fifth columns refer to the corresponding RSP standard deviations in the same ROI.

	mean		standard deviation	
	uniform	**FMpCT**	**uniform**	**FMpCT**
FF	0.992	-	0.047	-
0.5·FF	0.992	0.992	0.066	0.046
0.2·FF	0.992	0.990	0.109	0.044

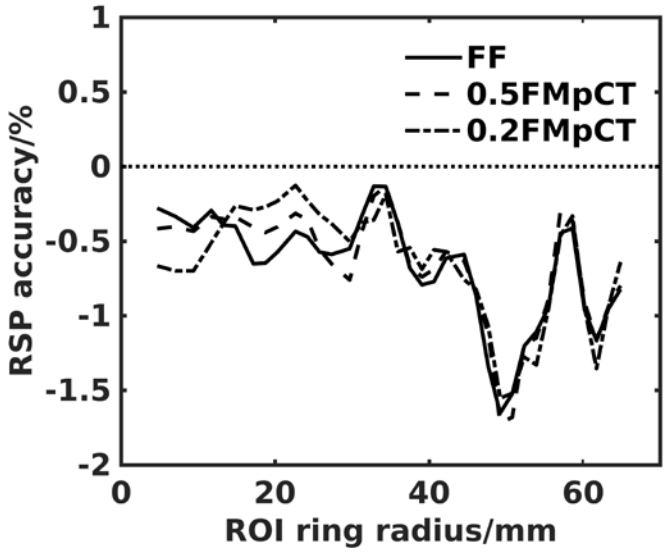

Figure 9. Error on mean RSP of water estimated from pCT images using annular ROIs.

Figure 10 presents the relative dose distributions, normalized to their maximum, of the FF and FMpCT scans. We observed the expected dose reduction outside the FMpCT-ROI when compared to the mostly uniform FF dose. At the object's edge, the imaging dose was 60% and 40% of the FF dose for FMpCT with FMF of 0.5 and 0.2 respectively, while in the center, the same dose was obtained for all cases. Due to the misaligned high fluence pattern, an intermediate 80% of FF dose halo was observed around the maximum dose region.

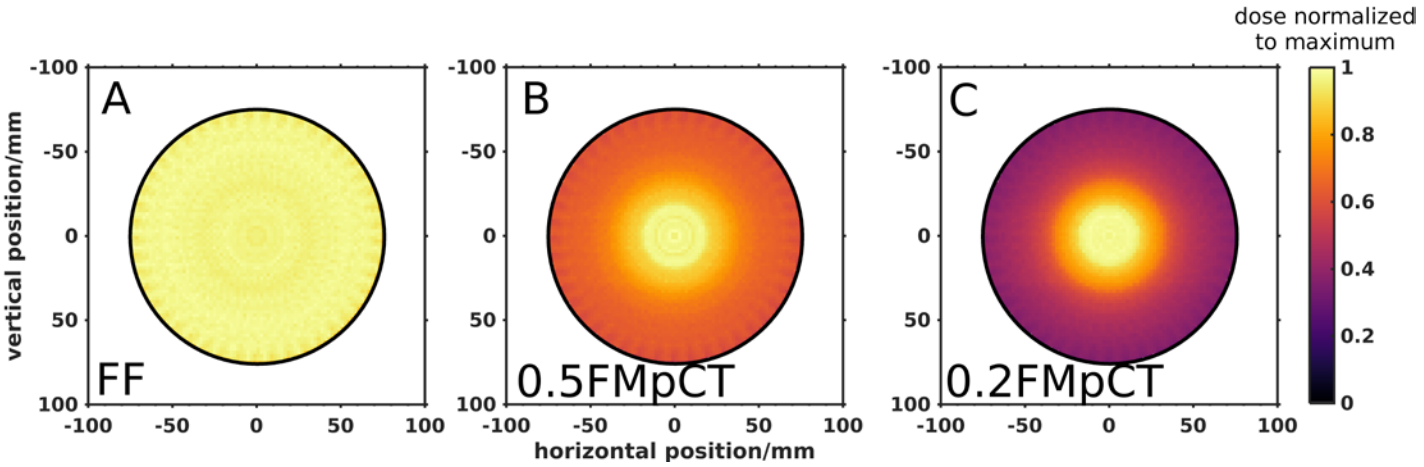

Figure 10. Normalized pCT scan doses in a central slice of the phantom (circumference indicated by dashed line). (A) Full fluence (FF), FMpCT with (B) FMF 0.5 and (C) FMF 0.2.

4. DISCUSSION

In this experimental study, we have demonstrated that the phase II pCT scanner prototype could be operated in PBS mode at acceptable pile-up levels. Previous mentions of scanner operation in proton PBS mode did not present pile-up analyses[28]. The chosen cyclotron current of 4 nA led to a scanner trigger rate of approximately 400 kHz. This was lower than the 1 MHz rate achievable with wobbled or cone beams[10]. In retrospect, even at the 1 MHz rate typically used with this scanner, the pile-up inefficiency would be acceptable. Although 96% hit efficiency would result in only 70% of protons being measured with all 8 hits, our analysis generally allows a single missing hit in both views, considerably reducing the impact of the inefficiency. Furthermore, when a phantom is placed in the beam, multiple scattering broadens the beam in the rear tracker, significantly reducing pile-up. Note that loss of single hits in the front tracker is relatively unimportant given that the incoming beam direction is well known.

The experiment was performed using slow step and shoot acquisition mode. The suggested increase in cyclotron current and pencil beam size might allow scan acquisition using continuous rotation.

We made use of a quarter PB spacing shift to interleave PBs from opposing projections, thus rendering the dose in a slice homogeneous. However, in the vertical dimension, interleaving is not possible and the dose distribution shows peaks and valleys corresponding to the PB pattern shown in Figure 6. It might be necessary to reduce the PB spacing in that direction to ensure homogeneous image quality.

The accuracy of the RSP for water was mostly within 1% for the PBS pCT scan, and comparable or better than what had been achieved with the wobbled beam. For both scan acquisition methods, we observed increasing noise with object radius. This is currently the subject of a separate investigation, and requires careful modelling of noise reconstruction in pCT as well as understanding of the various sources of projection noise, including detector effects. These might be modelled using the simulation platform of Giacometti et al.[14] The slightly higher noise levels at the object's edge observed with the wobbled beam may be caused by a fall-off of the fluence at the edge of the beam, however this has yet to be verified.

We were able to confirm the results of a previous simulation study suggesting that FMpCT should be feasible without loss of accuracy in the FMpCT-ROI[25]. We saw a very slight change (0.2%) in the water RSP when employing the 20% FMF. This appears consistent with the findings of Dedes et al.[25], where accuracy was degraded when using

FMF lower than 30% (see Figure 11 in that reference). The FF noise level in the FMpCT-ROI was preserved for both FMF, and we observed that the noise level outside the FMpCT-ROI approached the uniform low fluence results with increasing distance from the FMpCT-ROI. At a given FMF, the FMpCT scan noise was always lower than the uniform fluence scan noise since the full fluence PBs cross any given voxel at least once.

The relative dose reduction achieved in this study at 40% and 60% for FMF of 50 and 20 is comparable to what was achieved in the simulation study of Dedes et al.[25] Of course, these dose savings highly depend on the shape of the FMpCT-ROI. In this study, we opted for a simple central FMpCT-ROI, thus allowing us to neglect the synchronization of the PB fluence pattern and rotation angle. This was deemed sufficient for a proof-of-principle study, and next experiments will aim at performing FMpCT for arbitrarily shaped FMpCT-ROI. The unfortunate misalignment of the PB high fluence pattern meant that the dose falloff with distance from the FMpCT-ROI's edge was not as sharp as it could have been.

5. CONCLUSION

In this study, we have demonstrated that FMpCT scans are feasible. Furthermore, we have shown that PBS pCT scans can achieve equivalent accuracy as those obtained from broad beams. Image accuracy and noise were successfully preserved in the central FMpCT-ROI chosen for this study, and dose reduction of up to 60% at the object's edge was realized.

ACKNOWLEDGEMENTS

This work was supported by the German Research Foundation (DFG) project #388731804 “Fluence modulated proton computed tomography: a new approach for low-dose image guidance in particle therapy” and the DFG’s Cluster of Excellence Munich-Centre for Advanced Photonics (MAP), by the Bavaria-California Technology Center (BaCaTeC) and by the Bavaria-France Cooperation Centre (BFHZ). Dr. Valentina Giacometti is gratefully acknowledged for developing and sharing the Geant4 simulation platform used for dose calculation.

REFERENCES

1. Paganetti H. Range uncertainties in proton therapy and the role of Monte Carlo simulations. *Physics in medicine and biology.* Jun 7 2012;57(11):R99-117.
2. Yang M, Zhu XR, Park PC, et al. Comprehensive analysis of proton range uncertainties related to patient stopping-power-ratio estimation using the stoichiometric calibration. *Physics in medicine and biology.* Jul 7 2012;57(13):4095-4115.
3. Cormack AM. Representation of a Function by Its Line Integrals with Some Radiological Applications. *J Appl Phys.* 1963;34(9):2722-&.
4. Hansen DC, Sangild Sorensen T, Rit S. Fast reconstruction of low dose proton CT by sinogram interpolation. *Physics in medicine and biology.* Aug 7 2016;61(15):5868-5882.
5. Penfold SN, Rosenfeld AB, Schulte RW, Schubert KE. A more accurate reconstruction system matrix for quantitative proton computed tomography. *Med Phys.* Oct 2009;36(10):4511-4518.
6. Penfold SN, Schulte RW, Censor Y, Rosenfeld AB. Total variation superiorization schemes in proton computed tomography image reconstruction. *Med Phys.* Nov 2010;37(11):5887-5895.
7. Poludniowski G, Allinson N, Evans P. Proton computed tomography reconstruction using a backprojection-then-filtering approach. *Physics in medicine and biology.* 2014;59(24):7905.
8. Rit S, Dedes G, Freud N, Sarrut D, Letang JM. Filtered backprojection proton CT reconstruction along most likely paths. *Med Phys.* Mar 2013;40(3):031103.
9. Rinaldi I, Brons S, Gordon J, et al. Experimental characterization of a prototype detector system for carbon ion radiography and tomography. *Physics in medicine and biology.* Feb 7 2013;58(3):413-427.
10. Sadrozinski HFW, Geoghegan T, Harvey E, et al. Operation of the preclinical head scanner for proton CT. *Nuclear Instruments and Methods in Physics Research Section A: Accelerators, Spectrometers, Detectors and Associated Equipment.* 9/21/ 2016;831:394-399.

11. Taylor J, Poludniowski G, Price T, et al. An experimental demonstration of a new type of proton computed tomography using a novel silicon tracking detector. *Medical physics.* 2016;43(11):6129-6136.
12. Meyer S, Gianoli C, Magallanes L, et al. Comparative Monte Carlo study on the performance of integration-and list-mode detector configurations for carbon ion computed tomography. *Physics in medicine and biology.* 2017;62(3):1096.
13. Tanaka S, Nishio T, Tsuneda M, Matsushita K, Kabuki S, Uesaka M. Improved proton CT imaging using a bismuth germanium oxide scintillator. *Physics in medicine and biology.* 2018.
14. Giacometti V, Bashkirov VA, Piersimoni P, et al. Software platform for simulation of a prototype proton CT scanner. *Med Phys.* Mar 2017;44(3):1002-1016.
15. Schulte RW, Bashkirov V, Klock MC, et al. Density resolution of proton computed tomography. *Med Phys.* Apr 2005;32(4):1035-1046.
16. Bartolac S, Graham S, Siewerdsen J, Jaffray D. Fluence field optimization for noise and dose objectives in CT. *Medical physics.* Jul 2011;38 Suppl 1:S2.
17. Bartolac S, Jaffray D. Compensator models for fluence field modulated computed tomography. *Medical physics.* Dec 2013;40(12):121909.
18. Graham SA, Siewerdsen JH, Jaffray DA. Intensity-modulated fluence patterns for task-specific imaging in cone-beam CT. *P Soc Photo-Opt Ins.* 2007;6510:U16-U24.
19. Stayman JW, Mathews A, Zbijewski W, et al. Fluence-Field Modulated X-ray CT using Multiple Aperture Devices. *Proc Spie.* 2016;9783.
20. Szczykutowicz TP, Hermus J, Geurts M, Smilowitz J. Realization of fluence field modulated CT on a clinical TomoTherapy megavoltage CT system. *Physics in medicine and biology.* Sep 21 2015;60(18):7245-7257.
21. Szczykutowicz TP, Mistretta CA. Design of a digital beam attenuation system for computed tomography. Part II. Performance study and initial results. *Medical physics.* Feb 2013;40(2):021906.
22. Szczykutowicz TP, Mistretta CA. Design of a digital beam attenuation system for computed tomography: part I. System design and simulation framework. *Medical physics.* Feb 2013;40(2):021905.
23. Szczykutowicz TP, Mistretta CA. Experimental realization of fluence field modulated CT using digital beam attenuation. *Physics in medicine and biology.* Mar 07 2014;59(5):1305-1326.
24. Fuji H, Schneider U, Ishida Y, et al. Assessment of organ dose reduction and secondary cancer risk associated with the use of proton beam therapy and intensity modulated radiation therapy in treatment of neuroblastomas. *Radiation oncology.* 2013// 2013;8(1):255.
25. Dedes G, De Angelis L, Rit S, et al. Application of fluence field modulation to proton computed tomography for proton therapy imaging. *Physics in Medicine & Biology.* 2017;62(15):6026.
26. Meyer S, Magallanes L, Kopp B, et al. Tomographic imaging with carbon ion beams. Paper presented at: 2016 IEEE Nuclear Science Symposium, Medical Imaging Conference and Room-Temperature Semiconductor Detector Workshop (NSS/MIC/RTSD); Oct. 29 2016-Nov. 6 2016, 2016.
27. Magallanes Hernández L. *Low-dose ion-based transmission radiography and tomography for optimization of carbon ion-beam therapy*. Munich: Faculty of Physics, Ludwig-Maximilians-Universität München; 2017.
28. Volz L, Collins-Fekete C-A, Piersimoni P, et al. Stopping power accuracy and achievable spatial resolution of helium ion imaging using a prototype particle CT detector system. *Current Directions in Biomedical Engineering.* Vol 32017:401.

29. Johnson RP, Bashkirov V, DeWitt L, et al. A Fast Experimental Scanner for Proton CT: Technical Performance and First Experience With Phantom Scans. *Ieee T Nucl Sci.* Feb 2016;63(1):52-60.
30. Bashkirov VA, Schulte RW, Hurley RF, et al. Novel scintillation detector design and performance for proton radiography and computed tomography. *Med Phys.* Feb 2016;43(2):664-674.
31. Bashkirov VA, Johnson RP, Sadrozinski HF-W, Schulte RW. Development of proton computed tomography detectors for applications in hadron therapy. *Nuclear Instruments and Methods in Physics Research Section A: Accelerators, Spectrometers, Detectors and Associated Equipment.* 2016;809:120-129.
32. Johnson R, Bashkirov V, Coutrakon G, et al. Results from a Prototype Proton-CT Head Scanner. *Physics Procedia.* 2017;90:209-214.